Technical Notes

TECHNICAL NOTES are short manuscripts describing new developments or important results of a preliminary nature. These Notes cannot exceed 6 manuscript pages and 3 figures; a page of text may be substituted for a figure and vice versa. After informal review by the editors, they may be published within a few months of the date of receipt. Style requirements are the same as for regular contributions (see inside back cover).

A Mapped, Factored-Implicit Scheme for the Computation of Duct and Far-Field Acoustics

James W. White* and Peter E. Raad†
The University of Tennessee, Knoxville, Tennessee

Nomenclature

C_0^* = ambient speed of sound, m/s
f^* = frequency, Hz
H^* = characteristic duct dimension in transverse direction, m
P = dimensionless acoustic pressure, $=P^*/(\rho^* C_0^{*2})$
Q = grid control function
r = dimensionless radial coordinate, $=r^*/H^*$
R = dimensionless far-field boundary radius, R^*/H^*
S = grid control function
t = dimensionless time, $=t^* f^*$
X = dimensionless axial coordinate, $=X^*/H^*$
Y = dimensionless transverse coordinate, $=Y^*/H^*$
ξ,η = coordinates in transformed plane
ρ^* = ambient fluid density, kg/m^3
ω = dimensionless frequency, $=H^* f^*/C_0^*$
$(\ )^*$ = dimensional quantity

Introduction

WITH the increased emphasis on aircraft noise control during the past decade, more attention has been given to the development of numerical methods and computer codes for acoustic studies in complex geometries. A comprehensive comparison of various techniques currently used for solution of the sound propagation equations has been made by Baumeister.[1] This Note documents recent work in numerical duct acoustics that has been supported by NASA Lewis Research Center.

The new time-dependent, finite difference scheme that is the subject of this Note was developed with several specific objectives in mind. First, accurate implementation of the boundary conditions is very important due to the reflective nature of the hyperbolic equations governing noise propagation. Thus, one objective of the method is that the numerical solution should be developed around a general mapping procedure. A number of different approaches to numerical mapping may be found in the literature.[2] The present work generally follows the method developed by Thompson[2] and is based on defining the mapping by a pair of elliptic partial differential equations. Numerical solution of the mapping equations provides a grid system that is boundary fitted, with grid points that may be concentrated as desired on the boundary for high resolution. Use of such a general mapping procedure, together with an explicit acoustic algorithm, is described by White[3] for the analysis of noise propagation in a two-dimensional, variable-area duct. A second objective is that the algorithm should not require excessive computer memory, but at the same time should provide an accurate approximation of the acoustic field. In order to satisfy these requirements, a transient finite difference method together with a factored-implicit procedure was chosen.

Finally, the procedure should allow the noise calculation to proceed for some distance beyond the duct exit so that an appropriate acoustic boundary condition may be specified. This approach should be more accurate than terminating the calculation at the duct exit where only an approximate boundary condition can be specified. Also, information on the noise levels and radiation patterns emanating from the duct exit will be provided. In the sections that follow, the algorithm is briefly described and the numerical results of a test case are presented.

The Grid Mapping and Factored Acoustics Solver

The grid mapping is general and allows the boundaries to be irregular with steep curvature. Such mappings have been widely used for aerodynamics studies. The mapping equations are given by

$$\nabla^2 \xi = S(\xi,\eta) \tag{1a}$$

$$\nabla^2 \eta = Q(\xi,\eta) \tag{1b}$$

where ξ and η are the independent variables in the transformed plane and S and Q the "control terms" that may be specified in order to concentrate coordinate lines in the regions of special interest. The mapping is achieved by interchanging the dependent and independent variables in Eqs. (1) and solving the resulting equations in the transformed plane. Thompson[2] has reported problems of convergence in obtaining numerical mappings to complex geometries by successive-over-relaxation. In order to minimize such problems in the current work, the mapping equations are modified by adding time-derivative damping terms. The equations are then integrated in "time" with the desired mapping emerging asymptotically as the "steady-state" profile. The procedure has been reported by White[3] and seems to be a superior approach. Description of the acoustic propagation is accomplished by a spatially factored numerical scheme that is second-order time accurate in two dimensions, is noniterative, and requires the solution of only tridiagonal matrices.

In the computation of hyperbolic problems, considerable attention has recently been directed to the approximate treatment of infinite domains by using a truncated artificial boundary. In the present work, the following radiating boundary condition (due to Bayliss and Turkel[4]) is used on the truncated "far-field" boundary,

$$\omega \frac{\partial P}{\partial t} + \frac{\partial P}{\partial r} + \frac{P}{2r} = 0 \tag{2}$$

Received Dec. 5, 1983; presented as Paper 84-0501 at the AIAA 22nd Aerospace Sciences Meeting, Reno, Nev., Jan. 9-12, 1984; revision received April 9, 1984.

*Professor, Department of Mechanical and Aerospace Engineering.
†Graduate Assistant, Department of Mechanical and Aerospace Engineering. Member AIAA.

The purpose of the last term of Eq. (2) is to minimize reflections from the far-field boundary back into the computational domain.

For the case of two-dimensional zero mean flow, the linearized acoustic equations of momentum and continuity can be combined into a single wave equation for the pressure. After mapping, the transformed wave equation and boundary conditions are then cast into finite difference form and numerically integrated in time until a periodic steady state results. An excellent description of the factored-implicit approach to the solution of partial differential equations is given by Warming and Beam.[5]

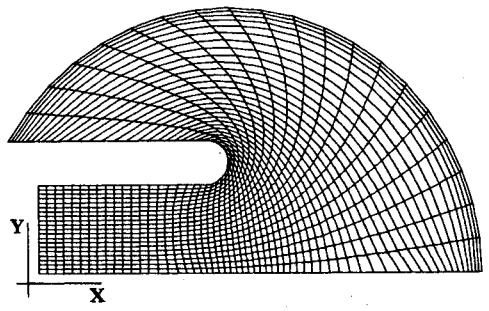

Fig. 1a Computational X-Y grid after mapping.

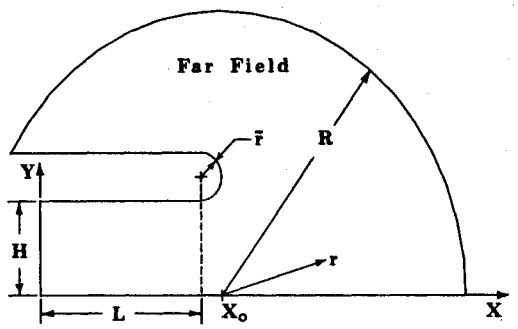

Fig. 1b Uniform area duct with far field (test case geometry: $L=2$, $H=1$, $\bar{r}=0.25$, $X_0=L+\bar{r}$, $R=3$).

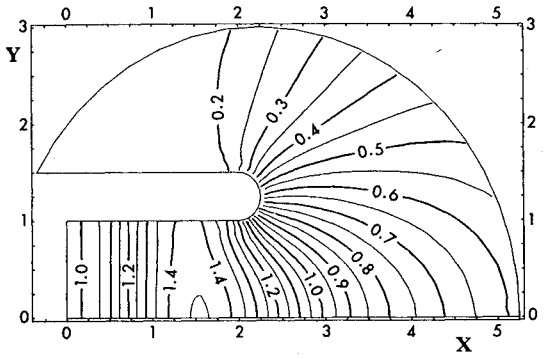

Fig. 2 Pressure contour plot for the geometry of Fig. 1b (hard-wall duct, $\omega=0.172$).

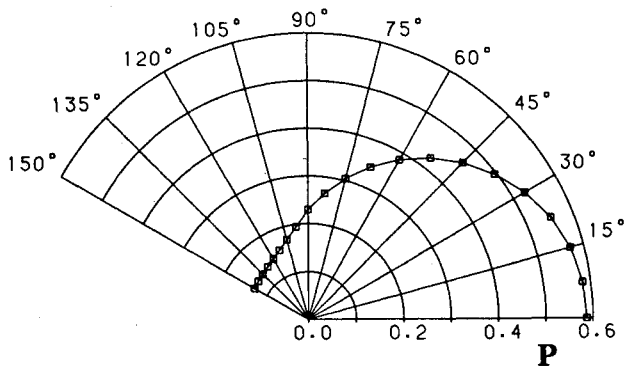

Fig. 3 Far-field pressure profile in polar coordinates.

The finite difference form of the transformed wave equation can be arranged to appear as

$$[1-L1(\xi)_{ij}][1-L2(\eta)_{ij}]\Delta P^n_{ij}=\phi_{ij} \tag{3}$$

where $L1$ and $L2$ are linear derivative operators.

The factored solution is achieved by rewriting Eq. (3) as

$$[1-L1(\xi)_{ij}]\Delta P^*_{ij}=\phi_{ij} \tag{4a}$$

$$[1-L2(\eta)_{ij}]\Delta P^n_{ij}=\Delta P^*_{ij} \tag{4b}$$

Equation (4a) represents a system of one-dimensional problems in the ξ direction, while Eq. (4b) represents a system of problems in the η direction. Each of these problems requires only a tridiagonal matrix inverse.

Numerical Results

The acoustic field was solved numerically over the 59×21 point grid of Fig. 1 for the case of a hard-wall duct. Computation was terminated at a "far-field" radius of three duct heights. The inlet noise source was uniform with a dimensionless frequency of 0.172. The numerical solution tracks the transient response from an initial condition until the pressure level throughout takes on a periodic steady state. Even though very small grid increments are used in some parts of the computational domain, the time step Δt did not suffer any grid size restriction, which allowed Δt to be chosen consistent with the physics of the problem.

A contour plot of the steady-state total pressure level is shown in Fig. 2 and the far-field pressure profile is shown in polar form in Fig. 3. Two interesting aspects of the solution are shown in Fig. 2. The duct pressure increases to about 1.45 (the absolute level of the noise source pressure is unity) before expanding into the far-field region. Also, it is observed that beyond the duct exit the pressure level does not generally follow a cylindrical expansion. The boundary condition used on the far field is strictly correct only for a cylindrical expansion, such as from a line noise source. Without the precisely correct boundary condition at every point on the far-field boundary, some energy incident on the far-field boundary will be reflected back into the computational domain and will persist in the solution as a steady-state error. In order to minimize such reflections, the far-field radius would have to be made much larger. This would be generally unacceptable, since the resulting memory and CPU requirements would become excessively large. A solution was also obtained for the case where the far-field radius is increased to six duct heights. The duct pressures are essentially the same as before, while the pressure levels beyond the duct exit (for a distance of about two duct heights) are on the order of 0.05 dimensionless units higher. It is concluded that for both cases ($R=3$ and 6), the influence of reflections from the far-field boundary back into the computational domain may have an influence on the steady-state results.

Conclusions

A mapped, factored-implicit numerical algorithm has been developed that should be useful for the calculation of duct and far-field acoustics. The mapping allows a very accurate implementation of boundary conditions, which is especially important for the calculation of the physics governed by hyperbolic differential equations over domains with irregular boundaries.

The factored-implicit scheme provides efficient computation without excessively small time steps and without the need

for large matrices. It has been demonstrated that the use of boundary conditions appropriate at a large distance from the duct exit may cause reflections and steady-state error when applied on an artificial truncated boundary at a moderate distance from the exit. Work is presently continuing on an iterative procedure for the far-field boundary condition. Primarily, it consists of treating the pressure at each point on the far-field boundary as locally one-dimensional. The boundary condition is applied so as to pass the one-dimensional pressure wave without reflection. A related approach has been used by Baumeister and Horowitz.[6] In their work, the acoustic impedance along the far-field boundary is iteratively adjusted to minimize reflection.

References

[1]Baumeister, K.J., "Numerical Techniques in Linear Duct Acoustics—A Status Report," *Journal of Engineering for Industry,* Vol. 103, No. 3, 1981, pp. 270-281.

[2]Thompson, J.F., "Numerical Solution of Flow Problems Using Body-Fitted Coordinate Systems," *Computational Fluid Dynamics,* Vol. 1, edited by W. Kollman, Hemisphere Publishing Corp., New York, 1980, pp. 1-98.

[3]White, J.W., "A General Mapping Procedure for Variable Area Duct Acoustics," *AIAA Journal,* Vol. 20, July 1982, pp. 880-884.

[4]Bayliss, A. and Turkel, E., "Radiation Boundary Conditions for Wave-Like Equations," *Communications on Pure and Applied Mathematics,* Vol. 33, 1980, pp. 707-725.

[5]Warming, R.F. and Beam, R.M., "On the Construction and Application of Implicit Factored Schemes for Conservation Laws," *SIAM-AMS Proceedings,* Vol. II, 1978, pp. 85-129.

[6]Baumeister, K.J. and Horowitz, S.J., "Finite Element-Integral Simulation of Static and Flight Fan Noise Radiation from the JT15D Turbofan Engine," NASA TM 82936, Nov. 1982.

Flow from Sharp-Edged Rectangular Orifices—The Effect of Corner Rounding

A. Pollard and M. A. Iwaniw†
Queen's University, Ontario, Canada

Introduction

THE free jet flows from sharp-edged rectangular orifices exhibit saddle-backed velocity distributions in the plane of the orifice major axis.[1-10] The maximum magnitude of these velocity excesses is typically 20% greater than the local mean centerline velocity (U_{ℓ}). Moreover, they occur in the region between the merging of the shear layers from the long sides of the orifice and the merging of the shear layers from the short sides of the orifice (i.e., $3 \leq x/t_p \leq 30$, for slot aspect ratio $\ell/t_p = 10$).

Although there has been, and continues to be, much discussion in the literature about the cause(s) for the occurrence of the saddle-backed velocity profile,[1-16] it is the author's opinion that no clear consensus has emerged. A reader interested in a comprehensive review of the literature is referred to Ref. 17.

In studies to date, the rectangular orifice plates have possessed sharp, 90-deg corner regions. These corner regions are, of course, the start of the interaction between the two sets of shear layers that originate along the short and long sides of the orifice. Although various gometrical alterations have been made to the orifices, such as upstream shaping[6] or the attachment of channels downstream of the orifice,[6,9] the effect of corner rounding on the appearance, magnitude, and location of these saddle-backed velocity distributions has not been addressed.

The purpose of this Note is to determine the effect of rounding the corners of a rectangular sharp-edged orifice on the location and magnitude of the saddle-backed velocity profiles. This is accomplished by reference to some previously published work[10,16] that used the same orifice but with sharp 90-deg corners (see Fig. 1).

Experiments

Laboratory air was supplied to a settling chamber by a fan. The rectangular orifice was attached to the downstream face of the settling chamber. This downstream face was flush with a large plywood wall to ensure that entrainment at the nozzle exit plane was normal to the jet centerline. The top and sides of the rig were covered with 1.59-mm mesh wire screen to prevent large-scale movement of air (room drafts) into the jet.

The experiments were performed in a $9.02 \times 7.39 \times 3.76$ m room into which traffic was strictly controlled. Check of ambient flow conditions verified the hypothesis that external disturbances and those produced by the jet itself were indeed very small.

The bilateral symmetry of the flow was utilized in acquiring data and checks were made to ascertain that symmetry did, in fact, exist in the two planes containing the major and minor axes of the orifice.

The orifices used are shown schematically in Fig. 1. These orifices were manufactured in accordance with British Standards for orifice plates (BS 1042). The sharp-corner orifice was made from four intersecting plates. The rectangular, sharp-edged, round-corner orifice is shown superimposed in the figure. Note that the area of the round-corner orifice is

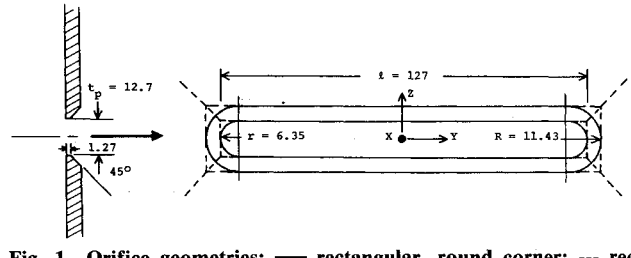

Fig. 1 Orifice geometries: — rectangular, round corner; --- rectangular, sharp corner.[10,16,17] (all dimensions in mm).

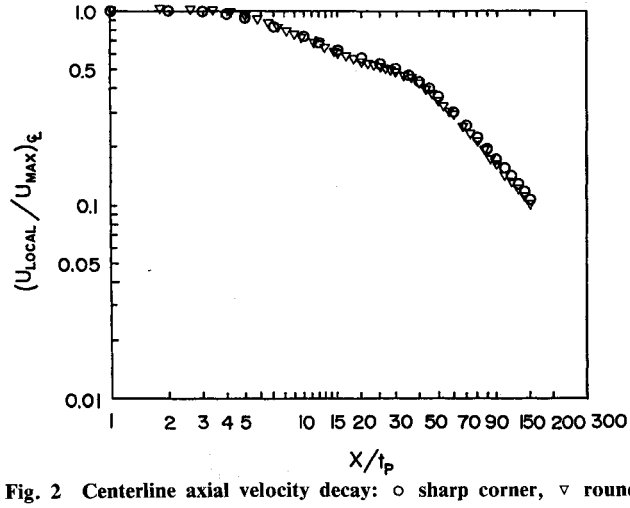

Fig. 2 Centerline axial velocity decay: ○ sharp corner, ▽ round corner.

Received Dec. 8, 1983; revision submitted April 23, 1984.

*Associate Professor, Department of Mechanical Engineering.
†Research Assistant, Department of Mechanical Engineering.